ICESat waveform measurements of within-footprint topographic relief and vegetation vertical structure

David J. Harding
Planetary Geodynamics Laboratory, NASA Goddard Space Flight Center, Greenbelt, Maryland, USA

Claudia C. Carabajal
NVI, Inc., Space Geodesy Laboratory, NASA Goddard Space Flight Center, Greenbelt, Maryland, USA

Received 11 May 2005; revised 8 July 2005; accepted 11 August 2005; published 15 October 2005.

[1] The Ice, Cloud and land Elevation Satellite (ICESat) mission determines land surface vertical structure within laser footprints due to topographic relief and vegetation using received waveforms recorded by the Geoscience Laser Altimeter System (GLAS). In low-relief areas with tree cover the waveforms and derived elevation products provide useful biophysical parameters, including maximum canopy height, crown depth, the outer-canopy ruggedness, and a measure of canopy cover. For areas where within-footprint topographic relief is large compared to vegetation height, interpretation of the waveforms is complex. The contribution of canopy and ground to received waveforms is illustrated by comparing them with co-located waveforms computed using an instrument model applied to high resolution Digital Elevation Models (DEMs). The model includes representations of the transmit pulse's spatial and temporal distributions, and the receiver field-of-view sensitivity and temporal smoothing. This provides a means to validate GLAS waveforms, elevation products, and footprint geolocation. **Citation:** Harding, D. J., and C. C. Carabajal (2005), ICESat waveform measurements of within-footprint topographic relief and vegetation vertical structure, *Geophys. Res. Lett.*, *32*, L21S10, doi:10.1029/2005GL023471.

1. Introduction

[2] The principal objectives of the Ice, Cloud and land Elevation Satellite (ICESat) mission are to measure: polar ice-sheet elevation change; atmospheric profiles of cloud and aerosol properties; land topography profiles referenced to a global datum; and height of vegetation canopies [*Zwally et al.*, 2002]. The objectives are accomplished using the Geoscience Laser Altimeter System (GLAS) [*Abshire et al.*, 2005] and precise orbit determination, with laser operations conducted in approximately month long periods three times a year [*Schutz et al.*, 2005]. Operations periods are designated by the laser used (1, 2, or 3) and sequential letters (a, b, c). GLAS received waveforms record 1064 nm wavelength laser energy as a function of time (Figure 1) reflected from footprints spaced 172 m apart along profiles. The footprint spatial distribution of energy for each laser pulse is recorded by the GLAS Laser Profiling Array (LPA) (J. M. Sirota et al., The transmitter pointing determination in the Geoscience Laser Altimeter System, submitted to *Geophysical Research Letters*, 2005, hereinafter referred to as Sirota et al., submitted manuscript, 2005). The footprints are elliptical, have central maxima, and an outward energy decrease. The ellipse size, where the energy is reduced to $1/e^2$ (13.5%) of the maxima, averaged 95 × 52 m for the Laser 1a through 2c periods and 61 × 47 m for the Laser 3a and 3b periods [*Abshire et al.*, 2005].

[3] After geolocation using orbit and laser pointing information, the waveforms provide the elevation distribution of illuminated surfaces within the footprint. Here attributes of waveforms and derived elevation products from vegetated terrain are described. GLAS waveforms are also compared to co-located waveforms computed using an instrument model applied to high-resolution, airborne laser altimeter digital elevation models (DEMs) in order to illustrate the contribution of vegetation and the ground to the signal.

2. GLAS Waveforms From Vegetated Land and Derived Elevation Products

[4] The "standard" ICESat elevation and associated latitude and longitude are reported in the products referred to as GLA06 and GLA12. They correspond to the centroid (distance-weighted average, or center of gravity) of a single Gaussian distribution, or the larger of two, fit to a waveform in order to identify large amplitude returns typical of flat ice sheets (A. C. Brenner et al., Geoscience Laser Altimeter System Algorithm Theoretical Basis Document: Derivation of Range and Range Distributions from Laser Pulse Waveform Analysis, 92 pp. in review, 2003, available at http://www.csr.utexas.edu/glas/atbd.html, hereinafter referred to as Brenner et al., in review, 2003). To accommodate more complex waveforms an "alternate" solution is reported for land areas and ice sheets in GLA14 (Figure 1). The alternate "signal start" and "signal end" are estimates of the highest- and lowest-detected surfaces within the footprint defined by first and last crossings of a low amplitude threshold. The alternate elevation corresponds to the centroid of the received waveform between signal start and end. An alternate model fit, the sum of up to six Gaussian distributions defined by their locations, amplitudes, and widths, provides a compact representation that identifies peaks in the waveform.

[5] Where topographic relief within a footprint is small compared to the vegetation height, tree-covered locations typically yield a bimodal GLAS waveform that can be used to estimate biophysical parameters (Figure 1). Reflections from plant surfaces and the underlying ground, where illuminated through canopy gaps, are separated vertically

0094-8276/05/2005GL023471$05.00

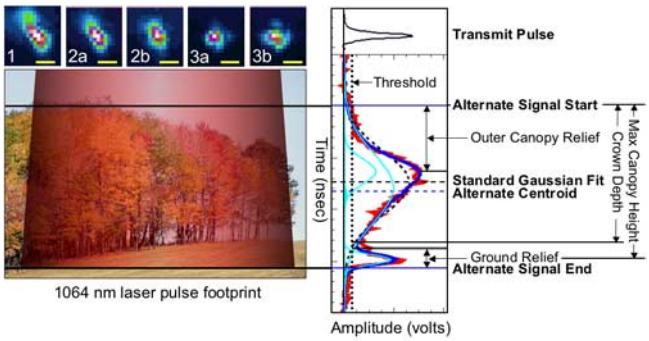

Figure 1. Representative Laser Profiling Array (LPA) images for five ICESat observation periods (top left; 1 = Laser 1, 2a = Laser 2a, etc.; energy color scale: black = 0, white = peak amplitude) and GLAS 1064 nm received waveform (right, red) typical of returns from tree cover on flat ground, the transmit pulse waveform which is 7 ns (∼1 m) wide at half the maximum amplitude (black), alternate threshold (dotted line), alternate signal start and end (horizontal blue lines) and centroid (horizontal dashed blue line), "standard" Gaussian fit and centroid (black dashed line), "alternate" fits (cyan), and alternate model fit from the sum of the alternate Gaussians (thick blue line). The received waveform and transmit pulse amplitudes are scaled separately. The tree cover depicted is illustrative; it does not correspond to the location of the waveform. The scale of the LPA images is indicated by the yellow lines, which are 50 m in length projected to the Earth's surface.

[*Harding et al.*, 2001]. Maximum canopy height, used as an estimate of above ground biomass [*Lefsky et al.*, 2005], corresponds to the distance between the signal start and the centroid of the ground return. The widths of the canopy and ground returns relative to the transmit pulse are measures of crown depth (canopy top to lowest major branch) and topographic relief. The distance from signal start to the peak of the canopy distribution is the result of the ruggedness of the upper-most canopy, the spatial organization of plant surfaces within the canopy, and the decrease in laser energy with depth into the canopy as the pulse is intercepted by plant surfaces. The ratio of canopy-to-total return energy is a measure of canopy cover (nadir-projected plant area versus total area), but it is dependent on the 1064 nm backscatter reflectance of plant surfaces and the ground [*Harding et al.*, 2001]. For areas where within-footprint topographic relief is a substantial fraction of the vegetation height, the canopy and ground reflections are mixed together making interpretation of the waveforms significantly more difficult.

[6] Several aspects of data acquisition and processing can introduce errors in the GLAS waveforms and derived products. In some cases, the threshold intersects background noise, causing signal start and/or signal end to be too high or low, respectively. The iterative, least-squares procedure (Brenner et al., in review, 2003) used to define alternate model fits produces results of varying quality, a small fraction of which are very poor. Fit quality is quantified by the standard deviation of differences between the model fit and received waveform. Through Release 21, this was computed on distributions scaled to volts, yielding results dependent on signal level. Future releases will use normalized distributions to achieve a measure fit quality comparable for all signal levels. Improvements to minimize the occurrence of poor fits are also being developed for future product releases.

[7] Where the return energy exceeds the linear response range of the receiver the GLAS waveforms become saturated and thus distorted (flat-topped and broadened, followed by an abrupt signal decrease and oscillations) [*Abshire et al.*, 2005]. To minimize occurrences of saturation, GLAS uses an automated detector gain adjustment. Rapid shot-to-shot change from low to high peak received energy (due to transitions from low to high reflectance, steep to flat relief, and/or cloudy to clear sky) can cause the gain to be too high, resulting in "high-gain" saturation. "Low-gain" saturation, where energy exceeds the receiver dynamic range at the lowest gain, is rare for vegetated landscapes. A measure of the degree of waveform saturation will be added to the GLA products post Release 21, augmenting flags that indicate the presence of low- and high-gain saturation. The high-gain flag, which has not been valid through Release 21, will be corrected for subsequent releases.

[8] For the Laser 1a and 2a periods, land waveform 1 ns sampling yielded an 81.6 m height range (544 waveform bins x ∼15 cm/bin). Because the acquisition software positions signal end within the waveform, this truncates the return from the upper part of tall vegetation and/or steep slopes. In these cases, signal start and the centroid underestimate the highest and average elevations. For subsequent operations periods a waveform compression scheme was implemented to increase the land height range to 150 m (lower 392 bins at 1 ns = 58.8 m; upper 151 bins averaged to 4 ns = 91.2 m). This significantly reduced occurrences of truncation.

3. Waveform Modeling Methodology

[9] To aid interpretation of GLAS waveforms and validate derived products, a waveform modeling capability was developed, expanding on the approach of *Blair and Hofton* [1999]. Model inputs are (1) the GLA04-01 20 × 20 LPA images of the transmit pulse spatial energy distribution (Sirota et al., submitted manuscript, 2005), (2) the GLA01 transmit pulse waveforms which account for the temporal distribution of laser energy and receiver band-pass smoothing [*Abshire et al.*, 2005], (3) a 44 × 44 image of the field-of-view (FOV) sensitivity for a detector of the same model as used in GLAS (X. Sun, personal communication, 2004), and (4) DEMs representing vegetated landscapes (full-feature) and the underlying ground (bald Earth). *Martin et al.* [2005] apply a similar method to DEMs of non-vegetated areas.

[10] Using parameters in the GLA-01, -05 and -06 products, LPA images were projected onto the Earth's surface with a scale factor of 16.4 μrad per pixel, oriented with respect to north, and positioned at the corresponding geolocation points (Figure 2). The detector sensitivity image was projected using a scale factor of 14.3 μrad per pixel, yielding a nominal FOV diameter of 380 m, with relatively uniform sensitivity across the center 60% and rapid decrease beyond.

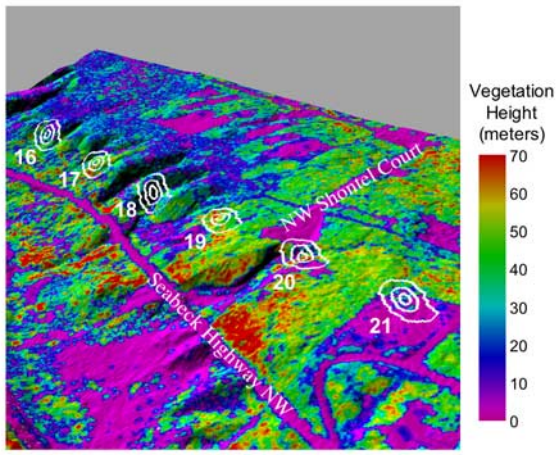

Figure 2. Hillshade perspective view of six GLAS footprints (Laser 2a, 8-day Track 43, Cycle 29, Release 21, record index 235611762, waveforms 16–21), with contours (white) corresponding to 12%, 50%, and 88% of the transmit pulse peak energy. Image color corresponds to vegetation height (full feature DEM minus bald Earth). The relief is bald Earth topography, vertically exaggerated by a factor of five.

It was oriented with respect to north using its alignment relative to the GLAS instrument axes (L. Ramos-Izquierdo, personal communication, 2004), and the spacecraft flight orientation and track azimuth. To simulate distortion of received waveforms due to transmit pulse to receiver misalignment (FOV shadowing), the FOV was displaced with respect to the GLAS footprint in the model.

[11] The full-feature and bald Earth DEMs were produced by TerraPoint, LLC for the Puget Sound Lidar Consortium using an airborne swath-mapping laser altimeter that records up to four discrete returns per pulse [*Haugerud et al.*, 2003]. Data used here are part of the Kitsap Peninsula, WA mapping acquired in February–March and December, 2000 (snow-free, leaf-off conditions) with sub-meter diameter footprints and a nominal density of one footprint per square meter. The DEMs have a grid spacing of six survey feet (1.83 m) with orthometric elevations referenced to NAVD-88 and easting and northing coordinates referenced to the Washington North State Plane Coordinate System, NAD83. ICESat footprint locations were converted to the DEM projection using Blue Marble's Geographic Calculator and the DEM elevations were converted to ellipsoidal values using GEOID-99 distributed by the National Geodetic Survey.

[12] The full-feature grid elevations were computed as a distance-weighted average of highest detected surfaces (i.e. first returns). The bald Earth grid elevations were sampled from a triangulated irregular network of last returns inferred to be from the ground using spatial filtering, thus removing vegetation cover and small buildings. The bald Earth DEM vertical accuracy was assessed by comparison to GPS survey points acquired at 22 non-vegetated, flat locations distributed randomly along roads across the Kitsap Peninsula; the mean and root-mean-square elevation errors are −3 cm and 23 cm.

[13] Model waveforms were generated by computing an elevation distribution of illuminated DEM pixels weighted using the LPA energy and FOV sensitivity images, with the total amplitude of each normalized to one. Backscatter 1064 nm reflectance was assumed to be constant for all pixels. The elevation distribution was smoothed by convo-

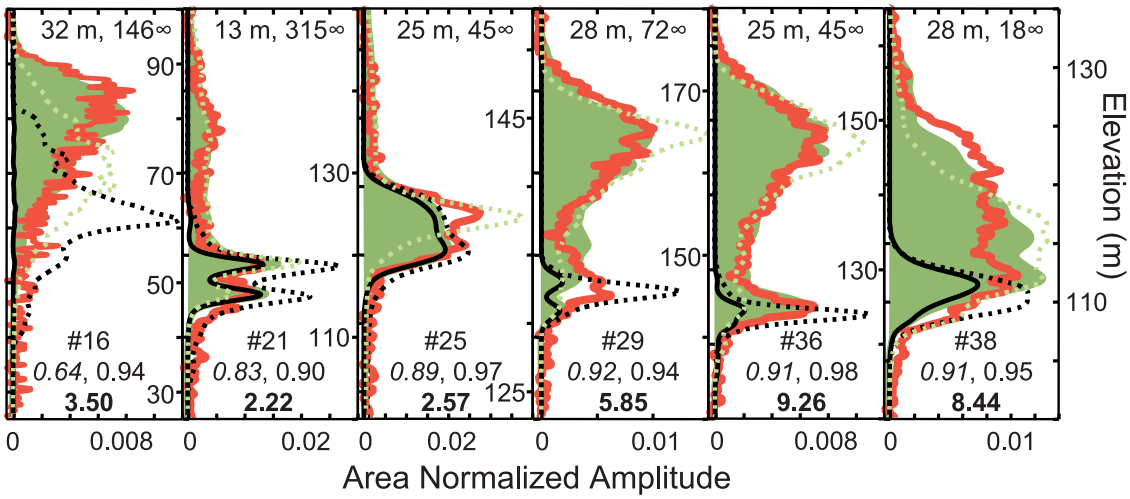

Figure 3. Received waveforms (red) and model waveforms derived from the full feature DEM at the geolocation point (dashed green), and the bald Earth DEM (dashed black), full feature DEM (filled green), and the portion of the full-feature DEM that is not vegetated (solid black) at the location of best match (record index 235611762, waveforms 16, 21, 25, 29, 36, and 38). The bald Earth amplitudes for waveforms 29, 36, and 38 are divided by 4, 5, and 3, respectively, to reduce the space required to display them. Values below the waveform numbers are Pearson's correlation coefficients between the received waveform and full-feature model waveforms at the geolocation point (italic) and location of best match, and received energy in fJ (bold). Receiver gain for shot 38 was 0.40 and was at its maximum (0.98) for the other shots. The magnitudes and azimuths of the shift to the best-match location are at the top of each plot.

lution with the transmit pulse waveform, converted from units of time to distance and normalized. No representation of instrument noise was included in the model. To evaluate ICESat geolocation accuracy, waveforms were computed at 121 locations, shifting the LPA and FOV easting and northing ±45.7 m centered about the geolocation point in increments of 9.1 m (5 DEM pixels). The "best match" was identified as the location where the correlation coefficient is maximized between the full-feature model waveform and received waveform, each with total amplitude normalized. Models run with and without FOV misalignment showed that, for vegetated landscapes, changes in waveform shape due to FOV shadowing and shifting of the footprint location were difficult to decouple. Therefore, for the results presented here, the FOV was centered on the footprint.

4. Waveform Modeling Results

[14] Received waveforms acquired in the Laser 2a period on September 30, 2003 (leaf-on conditions) from the Kitsap Peninsula exhibit a diversity of waveform types (Figure 3). In this area, relief is generally low but locally can be steep, and land cover includes cleared areas and mature and secondary re-growth forest stands of mixed coniferous and deciduous vegetation. For these waveforms, the signal was attenuated due to a low cloud layer 900 m above the ground surface, detected by the GLAS atmospheric lidar channel. This lowered received energies, to between 2.2 to 9.3 fJ, and signal-to-noise (S/N) ratios, compared to cloud-free land areas that typically yield received energies of 10 to 15 fJ. However, even for these low S/N examples the best-match model waveforms correspond closely to the received waveforms. The shifts to the best-match locations are mostly to the northeast, but do vary in direction and magnitude (Figure 3).

[15] Model waveforms for the bald Earth and non-vegetated portions of the full-feature DEM (pixels with elevations within 1 m of the bald Earth) clarify how the ground contributes to the signals. For example, bimodal waveforms 29 and 36 (Figure 3) correspond to tree cover on partially illuminated, relatively flat ground, with maximum vegetation heights of 30 and 35 m, respectively. Waveform 21 is from a sparsely vegetated location, with flat ground at two discrete elevations. Waveform 25 is from very sparsely vegetated ground of moderate relief that is uniformly distributed over a height range of approximately 7 m. Tree cover and moderate-relief ground are coalesced into a single broad (25 m) return in waveform 38. Waveform 16 is interpreted to be from a location with significant relief, where the vegetation cover is very dense and minimal signal is reflected from the ground.

5. Conclusion and Discussion

[16] The close correspondence to the modeled waveforms indicates that the received waveforms are an accurate representation of the distribution of surface heights within the GLAS footprints. Thus, estimation of biophysical parameters for tree-covered areas of low relief can be accomplished with ICESat. However, there is variability in the magnitude and direction of the best-match shifts. This variability could derive from several sources: (1) changes in vegetation cover between 2000 and 2003; (2) deciduous "leaf-off" versus "leaf-on" conditions; (3) different sensitivities to plant area of the discrete-return airborne altimeter as compared to the waveform-recording GLAS instrument; (4) absence of reflectance variations in the model; (5) no correction for the offset of the FOV with respect to the transmit pulse (which was present at the time these waveforms were acquired); (6) range delay due to atmospheric forward scattering caused by the low cloud layer through which these waveforms were acquired [*Duda et al.*, 2001] (the likely source of below-ground tails in the received waveforms that is most apparent in Waveform 38); or (7) shot-to-shot variation in geolocation error. Future modeling will use waveforms from cloud-free, non-vegetated, topographically-rugged areas when the FOV and transmit pulse were aligned, and airborne altimeter data that includes return intensity to estimate reflectance, in order to more precisely assess ICESat footprint horizontal geolocation accuracy. In addition, modeling of cloud-covered and cloud-free, non-vegetated, flat areas will be used to assess ranging errors introduced by saturation, FOV shadowing, and atmospheric forward scattering.

[17] **Acknowledgments.** This research was supported by NASA's ICESat Project and Terrestrial Ecology (RTOP 622-92-54) and Solid Earth and Natural Hazards (RTOP 613-78-32) programs. We thank the ICESat Science Project and the NSIDC for distribution of the ICESat data (see http://icesat.gsfc.nasa.gov and http://nsidc.org/data/icesat/). Marcos Sirota, David Mostofi, Charles Webb, Sungkoo Bae, Xiaoli Sun, and Louis Ramos-Izquierdo provided valuable assistance in implementing the instrument model. Comments by Helen Fricker, Chris Shuman, Bob Schutz and an anonymous reviewer improved the paper.

References

Abshire, J. B., et al. (2005), Geoscience Laser Altimetry System (GLAS) on the ICESat Mission: On orbit measurement performance, doi:10.1029/2005GL024028, in press.

Blair, J. B., and M. A. Hofton (1999), Modeling laser altimeter return waveforms over complex vegetation using high-resolution elevation data, *Geophys. Res. Lett.*, *26*, 2509–2512.

Duda, D. P., J. D. Spinhirne, and E. W. Eloranta (2001), Atmospheric multiple scattering effects on GLAS altimetry - part I: Calculations of single pulse bias, *IEEE Trans. Geosci. Remote Sens.*, *39*, 92–101.

Harding, D. J., M. A. Lefsky, G. G. Parker, and J. B. Blair (2001), Laser altimeter canopy height profiles: Methods and validation for deciduous, broadleaf forests, *Remote Sens. Environ.*, *76*, 283–297.

Haugerud, R., D. J. Harding, S. Y. Johnson, J. L. Harless, C. S. Weaver, and B. L. Sherrod (2003), High-resolution topography of the Puget Lowland, Washington—A bonanza for earth science, *GSA Today*, *13*, 4–10.

Lefsky, M. A., et al. (2005), Estimates of forest canopy height and above-ground biomass using ICESat, doi:10.1029/2005GL023971, in press.

Martin, C. F., et al. (2005), GLAS range and mounting bias estimation over precisely surveyed terrain, doi:10.1029/2005GL023800, in press.

Schutz, B., et al. (2005), Overview of the ICESat mission, doi:10.1029/2005GL024009, in press.

Zwally, H. J., et al. (2002), ICESat's laser measurements of polar ice, atmosphere, ocean, and land, *J. Geodyn.*, *34*, 405–445.

C. C. Carabajal, NVI, Inc., Space Geodesy Laboratory, NASA Goddard Space Flight Center, Code 697, Greenbelt, MD 20771, USA.

D. J. Harding, Planetary Geodynamics Laboratory, NASA Goddard Space Flight Center, Code 698, Greenbelt, MD 20771, USA. (david.j.harding@nasa.gov)